

Glancing-angle–deposited silica films for ultraviolet wave plates

S. MACNALLY,* C. SMITH, J. SPAULDING, J. FOSTER, AND J. B. OLIVER

Laboratory for Laser Energetics, University of Rochester, 250 East River Road, Rochester, NY 14623-1299, USA

*smacn@lle.rochester.edu

Abstract: Birefringent silica films are formed by glancing-angle deposition to fabricate quarter- and half-wave plates at a wavelength of 351 nm. A multilayer design is implemented to achieve low-loss transmittance with a high 351-nm laser-induced–damage threshold.

© 2019 Optical Society of America under the terms of the [OSA Open Access Publishing Agreement](#)

1. Introduction

The glancing-angle–deposition (GLAD) coating technique produces nanostructured columns that can easily be manipulated based on substrate orientation. These anisotropic structures create an artificial birefringence in the film, allowing for the creation of wave plates when depositing a film of the proper thickness. Compared to other methods of polarization control implemented in optical systems, the use of a deposited film is beneficial in the ability to improve laser-induced–damage thresholds (LIDT's), fabricate large-aperture components, and select from a diverse range of materials [1].

More-complex optical fields can be realized through the patterning of GLAD films. There has been an ongoing effort to develop a GLAD-based distributed polarization rotator (DPR) for use on the high-intensity National Ignition Facility (NIF) laser system. Spatially varying polarization states can help to reduce focal-point modulation in the system, providing polarization smoothing and more-uniform target illumination [1–5]. The goal of this experiment is to produce a low-loss, transmissive wave plate that can perform in a vacuum environment with a 351-nm, 5-ns incident laser pulse operating at a fluence of up to 12 J/cm² (satisfying NIF specifications). Silica was the selected material for this experiment since its high band-gap energy of ~9 eV correlates to a high LIDT [6].

Potential disadvantages of using GLAD for the creation of wave plates include the film's sensitivity to water vapor and the fact that the microstructure can introduce significant optical scatter, especially in thicker films [7–9]. Scatter can increase beam modulation, reducing the effectiveness of the DPR and potentially leading to damage initiation in optical components [10]. A multilayer technique to reduce scatter is explored in glancing-angle–deposited quarter- and half-wave plates, along with their dependence on humidity conditions. Coatings are demonstrated on fused-silica substrates up to 100 mm in diameter, and performance and uniformity are evaluated at 351 nm in both ambient and vacuum environments.

2. Background

GLAD is a coating process where the incident vapor condenses on a substrate oriented at a high incidence angle θ relative to the substrate normal. This high angle promotes self-shadowing from initially deposited material, forming columns that tilt toward the vapor source. The shadow regions extend behind these growing columns, creating a greater void percentage in the direction perpendicular to the substrate tilt axis [11]. With a lack of shadowing in the tilt-axis direction (x direction), there is a progressive fanning of the column cross-section into a somewhat elliptical shape, along with a chaining together of adjacent columns (as shown in Fig. 1). This shadowing asymmetry produces a biaxial film, where the film's refractive index is lower in the y direction than in the denser x direction [12].

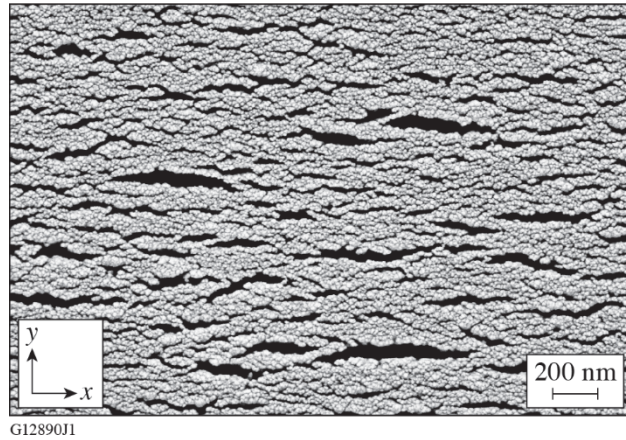


Fig. 1. Scanning electron microscope (SEM) image of the top of silica GLAD columns (coating surface). The substrate tilt axis is represented by x ; the shadowing/vapor source direction is represented by y . The coating thickness for this sample is $4 \mu\text{m}$.

Birefringence is created exclusively by this oriented-column morphology, rather than being a stress-related or intrinsic crystalline birefringence; the substrate angle and film thickness determine how much retardance will be present in the film at a specific wavelength [13]. To increase the birefringence of the film and improve uniformity, a serial bideposition process can be implemented, which involves alternating the deposition direction periodically between $\pm\theta$ rather than remaining at a fixed angle θ . This process creates anisotropic columns that are oriented perpendicular to the substrate [14,15].

GLAD allows for controlled refractive-index variations in a *single* material by tailoring the film porosity using the substrate deposition angle. An increasing substrate angle with respect to the incident vapor flux corresponds to an increasing shadow length, leading to greater void regions in the film and a lower average index of refraction. This technique is suitable for a wide range of materials and can achieve nearly any refractive index between the bulk material value and void regions (air) [13]. Conventional coating designs with alternating high- and low-index layers can be fabricated with a single desirable material, potentially improving the coating performance for a specific application. This approach has been successfully demonstrated with a wide variety of designs, including antireflection (AR), high reflection, and filter coatings [16–19].

To achieve the desired retardance for a quarter- or half-wave plate at 351 nm, the film thickness will be much greater than that of a typical AR coating. With the progressive fanning out and chaining together of individual columns during the growth process, an especially thick coating can lead to broader columns and greater light scattering in the film [13]. Another scatter-inducing property of GLAD films is the irreversible adsorption of water throughout the film's void regions when exposed to atmospheric water vapor [7,20]. The film's refractive indices decrease as water ($n = 1.3$) is removed from the film when transitioning from an ambient relative humidity (RH) to a vacuum environment (and vice versa), which is a common and reversible process with porous films [21]. However, as a GLAD sample is exposed to water vapor over time, water from the atmosphere will enter the film's pores, some of which will remain bonded to the film molecules, permanently altering the film structure and refractive indices. The ongoing adsorption of these water molecules is most likely contributing to additional column broadening/merging, which can increase optical scatter. Both column broadening and structural changes from water adsorption were observed in previous silica single-layer GLAD wave plates through scanning electron microscope (SEM) imaging and photometric measurements (10% to 15% optical scatter loss at 351 nm) [1].

Coating techniques to reduce column broadening include PhiSweep [22] and substrate swing [23], as well as a low substrate temperature during deposition [13]. A more recent technique uses an all-silica multilayer structure to limit column broadening [24]. Using a $\pm 70^\circ$ substrate angle, Grinevičiūtė *et al.* determined that the width of an individual, serial-bi-deposited silica column begins to increase beyond a 400-nm film thickness, more than doubling as the film thickness is increased to 1.5 μm . Their multilayer structure incorporates dense layers of silica throughout the coating (at intervals less than 400 nm) to stop the column growth before the inevitable width expansion. These dense layers are formed with the substrate perpendicular to the vapor source (0° substrate angle) and provide a base for the growth of a new birefringent layer. Individual layer thicknesses can be selected such that they remain “absentee” with respect to the use wavelength, having no net effect on the transmittance of the coating. This is true for layers that are an integer multiple of a half-wave optical thickness. This allows the two-layer structure to be repeated as many times as necessary to achieve the desired retardance for the wave plate. An AR coating can then be added as a final layer in the design [25].

Substrates can be patterned with these multilayer GLAD regions to provide spatially varying polarization states. Patterning methods might include translating the substrate behind an aperture during deposition [1], ion/chemical etching the film after deposition [26], or implementing a lift-off process with a pre-patterned optic [27].

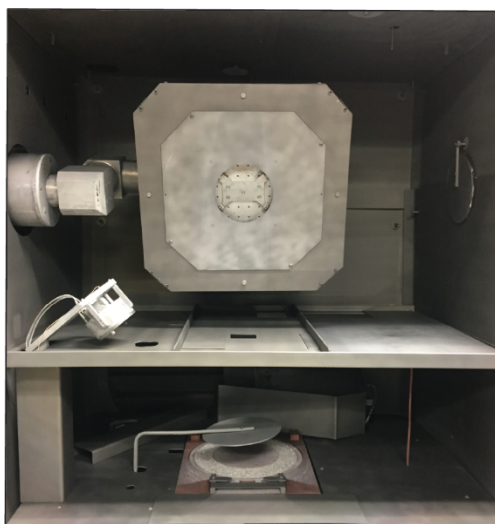
3. Experimental procedure

An optical coating design was developed to minimize transmission loss around 351 nm based on the layer grouping $(4B D)^x A$, where B is a birefringent layer, D is a dense layer, A is a birefringent antireflective layer, and x is the number of $(4B D)$ groupings; x will be determined for quarter- and half-wave plate designs based on measured retardance values. B , D , and A are quarter-wave optical thickness values at a 351-nm wavelength, with $4B$ representing a full-wave optical thickness. This structure is still considered to be absentee, even though D is not a multiple of a half-wave optical thickness, given that D has the same nominal refractive index as the substrate and therefore has a negligible effect on the optical performance of the component.

The GLAD coatings were deposited in a 1.2-m vacuum chamber using a trough-type EB Sources electron-beam gun with deposition rate and film thickness controlled by quartz crystal monitoring (as shown in Fig. 2). The chamber was heated with quartz lamps to 25°C and evacuated to approximately 1×10^{-6} Torr. Each coating deposition included a 100-mm-diam fused-silica substrate or two 50-mm-diam substrates: a silicon wafer and a fused-silica witness sample. The substrates were mounted on a custom Angstrom Engineering GLAD stage capable of tilt, rotation, and x/y scanning. Using serial bideposition, the stage rotated about the horizontal (substrate tilt) axis to the desired $\pm\theta$ every 6 s at a speed of $180^\circ/\text{s}$. Silica was evaporated at a rate of $9 \text{ \AA}/\text{s}$ as measured on the quartz crystal (without calibration for the variable substrate orientation) from a slowly rotating trough.

Since the refractive indices of these birefringent films change with substrate deposition angle and layer thickness, each layer in the multilayer design must be precisely calibrated. This required many short, single-layer depositions with various substrate angles and deposition times. A silicon wafer from each single-layer deposition was evaluated with a Woollam variable-angle spectroscopic ellipsometer (VASE[®]); these measurements were used to model refractive indices and thickness values. Additional measurement techniques were used to corroborate the ellipsometry data and more accurately determine the index and thickness of each layer. These include SEM film thickness measurements, a more advanced ellipsometry method with coupled measurement parameters, and an index/thickness calibration coating as described by Baumeister [11,28]. The calibration coating provided insight on how the refractive indices of individual layers change when used in a multilayer design. Some material from later dense layers may have been deposited between birefringent

columns, making the birefringent layer slightly more dense (higher refractive index) and the dense layer slightly less dense (lower refractive index). The coating transmittance was measured on a Lambda 900 spectrophotometer and fit to the original design in OptiRE, where the refractive indices and physical thicknesses were refined for *B* and *D* layers to more closely match the measured performance.



G12902J1

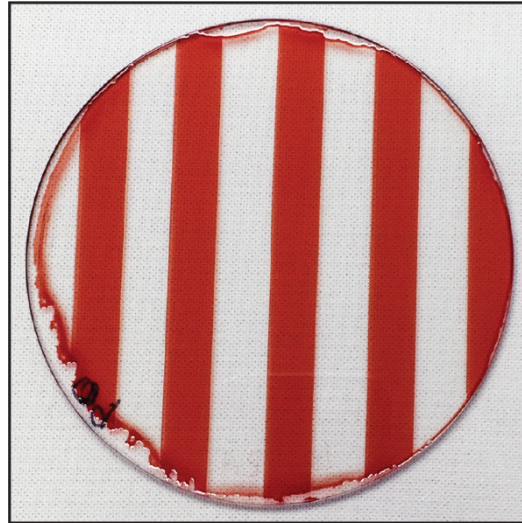
Fig. 2. Angstrom Engineering GLAD stage mounted in a 1.2-m vacuum chamber. Substrates remain in the center of the stage as it flips to the programmed $\pm\theta$. An electron-beam gun is mounted directly below the aperture, and an Inficon Crystal 12 sensor is mounted on the side to measure the deposition rate/thickness.

Reflectance and transmittance were measured using a 351-nm laser and a 4-in. integrating sphere with a silicon detector. The measurement system has a dual-beam ratioed configuration with a chopper and lock-in amplifier. The optical absorption of evaporated silica is negligible at a 351-nm wavelength, so any measured loss was considered to be the result of scatter from the film structure [29]. Retardance was measured with a Hinds Instruments Exicor[®] 450XT Mueller Matrix Polarimeter at a wavelength of 355 nm. Every *4B* layer has the same nominal retardance, so a simple calculation is needed to determine the number of (*4B D*) groupings for each wave plate design in order to approach the desired retardance (87.75 nm for the quarter-wave plate and 175.5 nm for the half-wave plate at 351 nm). Laser-damage testing for the quarter-wave plate design was performed on polished fused silica processed with an “advanced mitigation process” (AMP) using a 400- μm -diam, 1-ns pulse at 351 nm [30,31]. The LIDT of this uncoated AMP substrate is $40.35 \pm 1.10 \text{ J/cm}^2$ in a 1:1 testing protocol (one shot per site) and $44.15 \pm 13.53 \text{ J/cm}^2$ in an *N*:1 testing protocol (gradually ramped fluence over multiple shots for a single site).

Because the adsorption of water can alter the refractive indices and retardance of a GLAD film, all measurement techniques were performed in an environmental enclosure. These stable measurement conditions allowed for more-accurate calibrations, better comparisons between coating depositions, and the ability to evaluate all aspects of the film in its final use environment (0% RH). Variations in individual measurements were tracked both over time and between ambient and nitrogen-purged environments.

The selected method of patterning was a lift-off process using photolithography. Fused-silica substrates, 100 mm in diameter, were prepared with vertical stripes of photoresist

prior to deposition in the vacuum chamber. The substrates were first coated with $9\ \mu\text{m}$ of positive photoresist and then holographically exposed using an optic patterned with stripes of lithography tape as a mask. Exposed areas of photoresist were then removed with developer, leaving the unexposed stripes of photoresist on the substrate. One of these striped substrates is shown in Fig. 3. This substrate was mounted in the vacuum chamber and a half-wave plate coating (minus the final AR layer) was deposited across the entire 100-mm surface. The coated optic was then placed in acetone until all photoresist was removed (~ 13 min). The final AR layer will be deposited across the 100-mm surface.



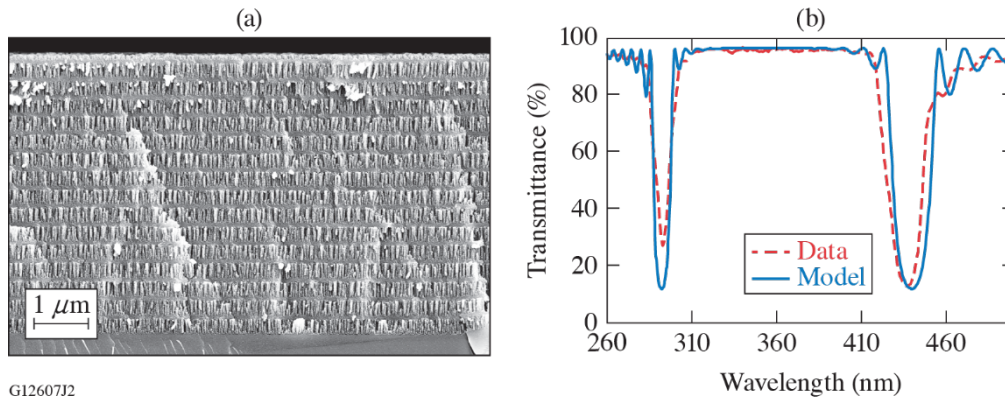
G12891J1

Fig. 3. A 100-mm fused-silica substrate with stripes of photoresist. The stripes are 10 mm wide (the width of the lithography tape used to pattern the exposure mask) and are evenly spaced across the surface.

4. Results and discussion

After many single-layer and multilayer calibration depositions, accurate thickness data and dispersion curves (n_x , n_y , and n_z) were acquired in a vacuum environment for each layer in the wave plate design. For modeling purposes, the refractive index value used for the birefringent layers was an average of the measured n_x (shadowing direction) and n_y (tilt-axis direction) at a 351-nm wavelength. The $4B$ layers were deposited with the substrate at 73° and have an average index of 1.29, the top AR layer was deposited at 82° and has an average index of 1.21, and the dense layers were deposited with the substrate perpendicular to the vapor source (0° substrate angle) and have an index of 1.46. Coating thickness was measured with a SEM and found to be $5.2\ \mu\text{m}$ for the quarter-wave plate (~ 2.5 -h deposition time) and $10.5\ \mu\text{m}$ for the half-wave plate (~ 5 -h deposition time). The thickness of each $4B$ layer (~ 270 nm) did not exceed the 400-nm value where column broadening begins to occur for silica GLAD columns [24].

Photometric performance was evaluated with a 351-nm laser at a distance of 350 mm. The quarter-wave plate exhibited a reflectance of 3.9% and a transmittance of 95.8%, yielding a loss of 0.3%, while the half-wave plate exhibited a reflectance of 4.2 % and a transmittance of 95.3%, yielding a loss of 0.5%. Both reflectance measurements include the uncoated back surface of the substrate. Transmittance was also measured on a spectrophotometer, as shown in Fig. 4. These results closely match the theoretical transmittance with backside reflection.

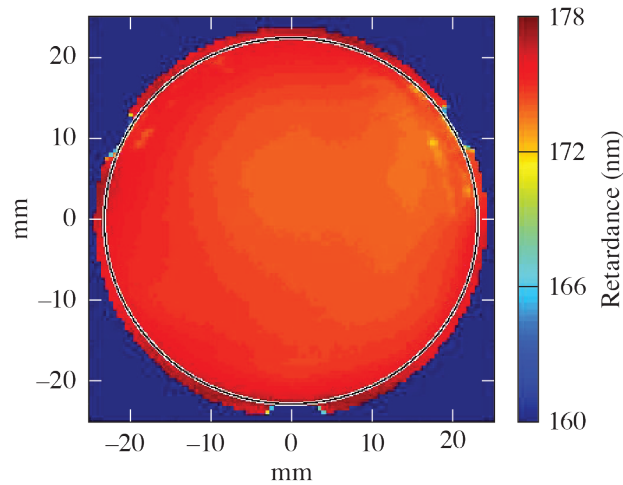


G12607J2

Fig. 4. (a) SEM image of a 31-layer quarter-wave plate coating. (b) Theoretical transmittance through the quarter-wave design with backside reflection (solid line) overlaid with spectrophotometer data (dashed line).

The LIDT for a multilayer, quarter-wave plate coating on the AMP substrate was found to be $12.51 \pm 0.51 \text{ J/cm}^2$ in a 1:1 testing protocol and $36.31 \pm 3.74 \text{ J/cm}^2$ in an $N:1$ testing protocol. This is an improvement from previous silica single-layer LIDT measurements ($\sim 11 \text{ J/cm}^2$ in both a 1:1 and $N:1$ testing protocol) [1].

Retardance was found to be uniform across all 50-mm and 100-mm samples. A retardance map for one of the 50-mm half-wave plate samples is shown in Fig. 5. The average retardance measurement across this 50-mm sample is $174.60 \text{ nm} \pm 0.62 \text{ nm}$, while the average measurement across a 100-mm sample was found to be $175.58 \text{ nm} \pm 0.98 \text{ nm}$.



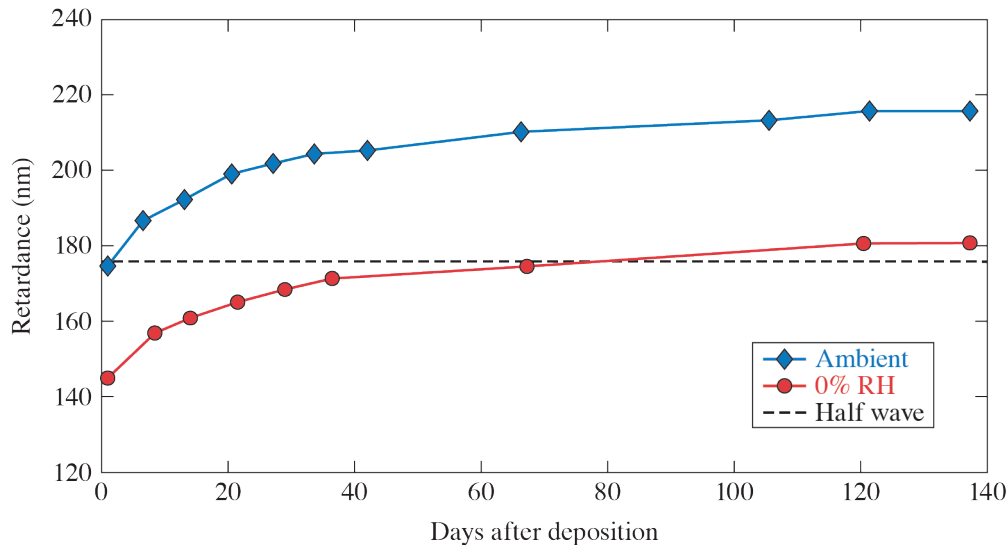
G12892J1

Fig. 5. Retardance map of a 50-mm-diam multilayer half-wave plate measured on a Hinds Instruments Exicor[®] 450XT Mueller Matrix Polarimeter. The resolution of this measurement tool is 0.5 mm and the measurement wavelength is 355 nm.

Retardance was measured in both an ambient and nitrogen-purged (0% RH) environment. For each single-layer and multilayer sample, the measurement in vacuum was 20% to 25% lower than the ambient measurement. This change is reversible when cycling through

environments and is due to the removal/introduction of water inside the film pores [21]. Since these films will eventually be used in a vacuum environment, the number of $4B$ layers in the final design (determining the overall thickness) was based on the single-layer, *nitrogen-purged* measurements. As with the refractive indices, retardance changed slightly when a single layer was placed in a multilayer stack. The measured retardance for quarter- and half-wave plates was 5% to 7% lower than expected, based on the single-layer measurements, and additional ($4B D$) groupings were added to each wave-plate design.

In addition to a retardance change between environments, there was also a change observed over time. The retardance values for single-layer and multilayer wave plates (both ambient and vacuum) had increased $\sim 17\%$, one month after deposition. Because of this projected increase across all samples, coatings were designed to have $\sim 20\%$ less than the desired retardance (accomplished with fewer groupings of birefringent and dense layers). With continual retardance monitoring of the samples, there has been an increase of $\sim 24\%$ in both ambient and vacuum environments, five months after deposition. The coating design thickness, and in turn deposition time, will continue to decrease with future retardance monitoring until the retardance stabilizes at the desired value and the percent increase is known. Retardance values for a multilayer half-wave plate sample (initially designed for a 20% increase) are shown in Fig. 6.



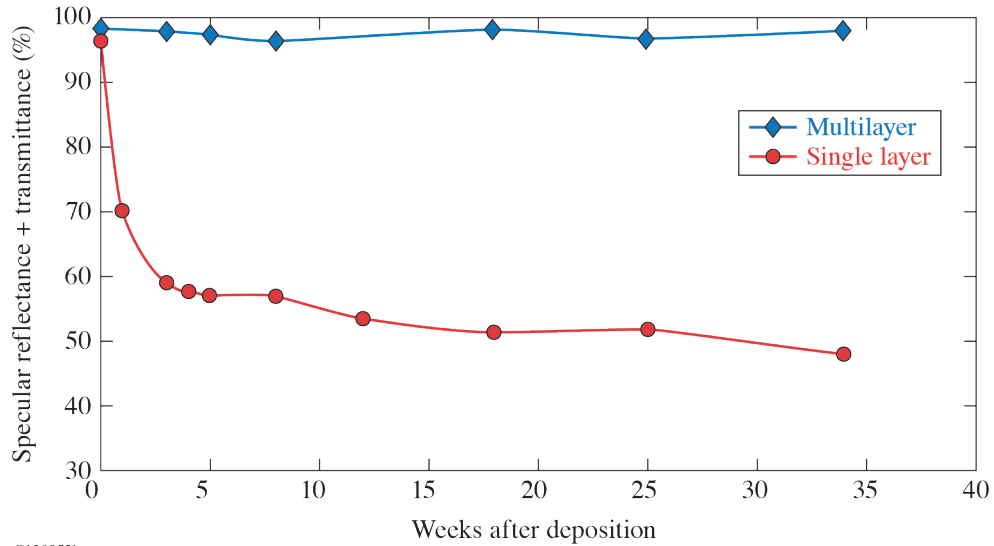
G12893J1

Fig. 6. Retardance measurements for a half-wave plate sample over a five-month period. Ambient measurements are consistently $\sim 20\%$ higher than nitrogen-purged measurements.

It is hypothesized that this gradual increase in retardance is due to the irreversible adsorption of atmospheric water vapor. This change occurred with vacuum measurements as well because the wave plates were stored in an ambient environment between measurements. Routine retardance monitoring will continue for both single-layer and multilayer wave plates until values have stabilized. Future experiments will be performed to further test this hypothesis, one of which will involve controlling the environment where the two coated substrates per run are stored. One sample will be exposed to atmosphere, and the other will always remain in a vacuum environment (potentially preventing a retardance increase over time).

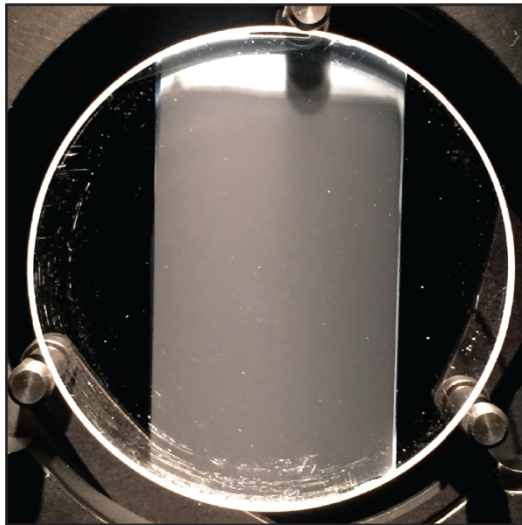
Percent scatter is another data set found to increase over time, also most likely a result of the film's susceptibility to water in the atmosphere. A significant increase was observed in

single-layer samples, more so in thicker coatings. Eight months after deposition, the scatter detected in single-layer quarter- and half-wave plate samples increased 16% and 48%, respectively, while the scatter increase in multilayer wave plates remained under 1% (Fig. 7). The introduction of scatter in the single-layer samples can be visibly detected from the now-frosted appearance of the coating. An image of a single-layer sample (five months after deposition) is shown in Fig. 8.



G12895J1

Fig. 7. Scatter measurements for a single-layer and multilayer half-wave plate. Eight months after deposition, multilayer scatter has remained approximately the same and single-layer scatter has increased 48%.



G12894J1

Fig. 8. Image of a single-layer GLAD stripe on a 50-mm substrate, five months after deposition. The coating thickness is 4 μm .

As previously discussed, this scatter increase over time in single-layer GLAD coatings is most likely caused by the recurrent bonding of water molecules to the film structure, contributing to additional column broadening and merging. Column features (individual diameters and those of columns now chained together) begin to approach the wavelength of light at the film thicknesses necessary to achieve a quarter- and half-wave of retardance at 351 nm. With these features already providing a means of scatter, the changing film structure with the addition of water molecules would only amplify the amount of scatter measured in the film. Since the multilayer technique limits column broadening during film growth, the structural changes caused by the ongoing addition of water molecules are insufficient to create features large enough to cause scatter.

The lift-off process was successful in patterning a 100-mm optic with stripes of multilayer GLAD regions, and the photometric performance and retardance uniformity were evaluated. Figure 9 includes an image of a half-wave plate coating, along with the corresponding retardance map. The average retardance of the GLAD stripes was measured to be $163.41 \text{ nm} \pm 1.15 \text{ nm}$. This retardance value is slightly lower than that of an unpatterned half-wave plate because the photoresist thickness, and therefore GLAD coating thickness, was limited by the type of photoresist available for this experiment. Layer groupings were intentionally removed from the GLAD coating design to accommodate this limitation.

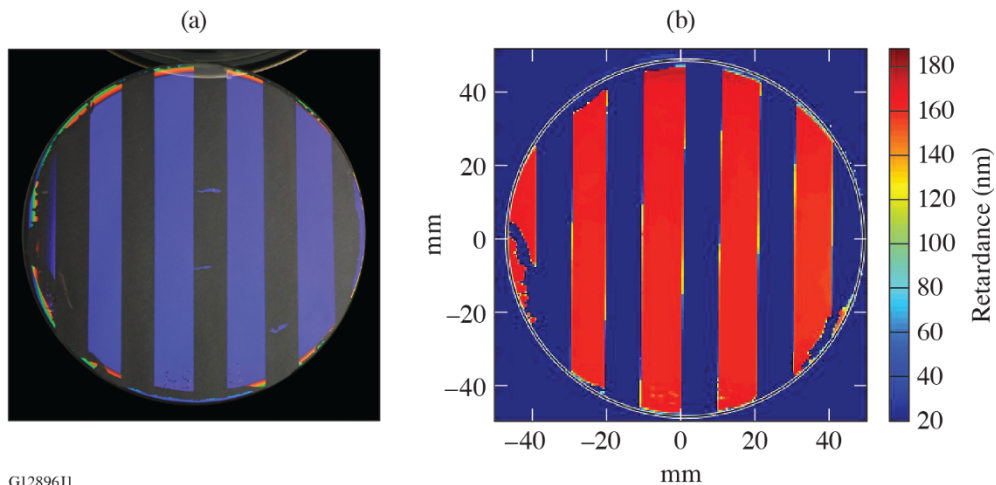
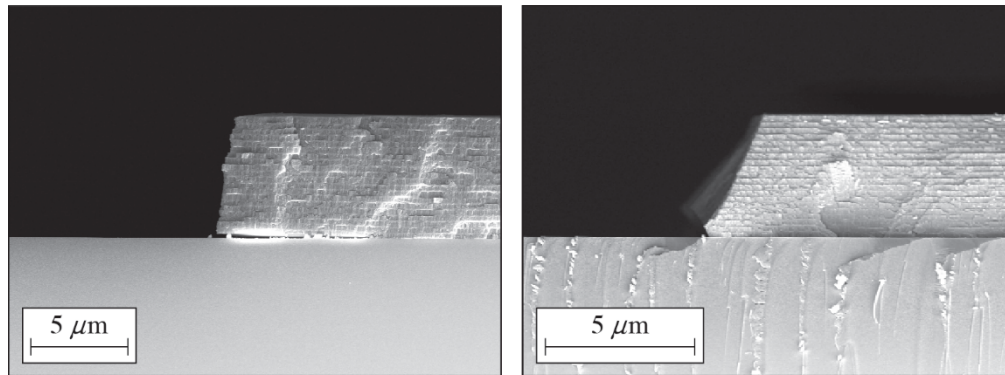


Fig. 9. (a) Image of the 100-mm patterned optic. (b) The retardance map shows uniformity across the 100-mm sample.

This half-wave plate coating exhibited a reflectance of 8.3% and a transmittance of 90.8%, yielding a loss of 0.9%. The AR layer is yet to be deposited on this patterned optic, but when that final step is complete, reflectance and transmittance values should be similar to those for the unpatterned half-wave plate. SEM images of various stripe edges are shown in Fig. 10.



G12897J1

Fig. 10. SEM images of the 40-layer, patterned GLAD coating.

5. Conclusions

Quarter- and half-wave plates were successfully fabricated and patterned for use at 351 nm in a vacuum environment. The all-silica multilayer structure has a low loss, high LIDT, and wide design bandwidth. The insertion of dense layers throughout the coating limited column broadening during the film growth as well as over time, preventing a significant increase of optical scatter in the film. With future retardance monitoring, an exact design thickness for each wave plate can be realized as the retardance values stabilize in all humidity conditions. The effects of water adsorption on the film structure will also be further investigated.

Funding

This material is based upon work supported by the Department of Energy National Nuclear Security Administration under Award Number DE-NA0003856, the University of Rochester, and the New York State Energy Research and Development Authority.

Acknowledgment

The authors express their appreciation to Brittany Hoffman for the LIDT measurements.

This report was prepared as an account of work sponsored by an agency of the U.S. Government. Neither the U.S. Government nor any agency thereof, nor any of their employees, makes any warranty, express or implied, or assumes any legal liability or responsibility for the accuracy, completeness, or usefulness of any information, apparatus, product, or process disclosed, or represents that its use would not infringe privately owned rights. Reference herein to any specific commercial product, process, or service by trade name, trademark, manufacturer, or otherwise does not necessarily constitute or imply its endorsement, recommendation, or favoring by the U.S. Government or any agency thereof. The views and opinions of authors expressed herein do not necessarily state or reflect those of the U.S. Government or any agency thereof.

Disclosures

SCM: None, CCS: None, JES: None, JPF: None, JBO: Vacuum Innovations LLC (I, E).

References

1. J. B. Oliver, T. J. Kessler, C. Smith, B. Taylor, V. Gruschow, J. Hettrick, and B. Charles, "Electron-beam-deposited distributed polarization rotator for high-power laser applications," *Opt. Express* **22**, 23,883–23,896 (2014).
2. D. H. Munro, S. N. Dixit, A. B. Langdon, and J. R. Murray, "Polarization smoothing in a convergent beam," *Appl. Opt.* **43**, 6639–6647 (2004).

3. J. E. Rothenberg, "Polarization beam smoothing for inertial confinement fusion," *J. Appl. Phys.* **87**, 3654–3662 (2000).
4. S. Skupsky and R. S. Craxton, "Irradiation uniformity for high-compression laser-fusion experiments," *Phys. Plasmas* **6**, 2157–2163 (1999).
5. S. N. Dixit, D. Munro, J. R. Murray, M. Nostrand, P. J. Wegner, D. Froula, C. A. Haynam, and B. J. MacGowan, "Polarization smoothing on the National Ignition Facility," *J. Phys. IV France* **133**, 717–720 (2005).
6. B. Mangote, L. Gallais, M. Zerrad, F. Lemarchand, L. H. Gao, M. Commandre, and M. Lequime, "A high accuracy femto-/picosecond laser damage test facility dedicated to the study of optical thin films," *Rev. Sci. Instrum.* **83**, 013109 (2012).
7. L. González-García, J. Parra-Barranco, J. R. Sánchez-Valencia, A. Barranco, A. Borrás, A. R. González-Elipse, M.-C. García-Gutiérrez, J. J. Hernández, D. R. Rueda, and T. A. Ezquerro, "Correlation lengths, porosity and water adsorption in TiO₂ thin films prepared by glancing angle deposition," *Nanotechnology* **23**, 205701 (2012).
8. S. Kassam, I. J. Hodgkinson, Q. Wu, and S. C. Cloughley, "Light scattering from thin films with an oblique columnar structure and with granular inclusions," *J. Opt. Soc. Am. A* **12**, 2009–2021 (1995).
9. T. A. Germer, K. A. Sharma, T. G. Brown, and J. B. Oliver, "Polarized optical scattering by inhomogeneities and surface roughness in an anisotropic thin film," *J. Opt. Soc. Am. A* **34**, 1974–1984 (2017).
10. K. A. Sharma, T. A. Germer, C. Smith, J. D. Zuegel, J. B. Oliver, and T. G. Brown, "Scattered-light analysis of birefringent coatings for distributed polarization rotators," in *Frontiers in Optics 2016*, OSA Technical Digest (online) (Optical Society of America, 2016), p. Paper JW4A.48.
11. C. Smith, S. MacNally, and J. B. Oliver, "Modeling of serially bi-deposited glancing-angle-deposition coatings," submitted to *Applied Optics*.
12. M. W. McCall, I. J. Hodgkinson, and Q. Wu, *Birefringent Thin Films and Polarizing Elements*, 2nd ed. (Imperial College, 2015), pp. 4,5.
13. M. M. Hawkeye, M. T. Taschuk, and M. J. Brett, *Glancing Angle Deposition of Thin Films: Engineering the Nanoscale*, Wiley Series in Materials for Electronic & Optoelectronic Applications (Wiley, 2014), pp. 6,7, 53–60, 237–240.
14. I. Hodgkinson and Q. H. Wu, "Serial bideposition of anisotropic thin films with enhanced linear birefringence," *Appl. Opt.* **38**, 3621–3625 (1999).
15. I. J. Hodgkinson, "Linear and circular form birefringence of coatings fabricated by serial bideposition," *Proc. SPIE* **3790**, 119–132 (1999).
16. S. R. Kennedy and M. J. Brett, "Porous broadband antireflection coating by glancing angle deposition," *Appl. Opt.* **42**, 4573–4579 (2003).
17. J. Q. Xi, M. F. Schubert, J. K. Kim, E. F. Schubert, M. Chen, S.-Y. Lin, W. Liu, and J. A. Smart, "Optical thin-film materials with low refractive index for broadband elimination of fresnel reflection," *Nature Photon.* **1**, 176–179 (2007).
18. K. Kaminska, T. Brown, G. Beydaghyan, and K. Robbie, "Vacuum evaporated porous silicon photonic interference filters," *Appl. Opt.* **42**, 4212–4219 (2003).
19. K. Kaminska and K. Robbie, "Birefringent omnidirectional reflector," *Appl. Opt.* **43**, 1570–1576 (2004).
20. S. J. Gregg and K. S. Sing, *Adsorption, Surface Area and Porosity*, London: Academic Press (1982), pp. 269–274.
21. S. F. Pellicori and H. L. Hettich, "Reversible spectral shift in coatings," *Appl. Opt.* **27**, 3061–3062 (1988).
22. M. O. Jensen and M. J. Brett, "Porosity engineering in glancing angle deposition thin films," *Appl. Phys. A* **80**, 763–768 (2005).
23. D. X. Ye, T. Karabacak, R. C. Picu, G. C. Wang, and T. M. Lu, "Uniform Si nanostructures grown by oblique angle deposition with substrate swing rotation," *Nanotechnology* **16**, 1717–1723 (2005).
24. L. Grinevičiūtė, A. Andrulevičius, A. Melninkaitis, R. Buzelis, A. Selskis, A. Lazauskas, and T. Tolenis, "Highly resistant zero-order waveplates based on all-silica multilayer coatings," *Phys. Stat. Sol. A* **214**, 1770175 (2017).
25. J. B. Oliver, S. MacNally, C. Smith, B. N. Hoffman, J. Spaulding, J. Foster, S. Papernov, and T. J. Kessler, "Fabrication of a glancing-angle-deposited distributed polarization rotator for ultraviolet applications," *Proc. SPIE* **10691**, 106911C (2018).
26. K. D. Harris, "Fabrication and applications of highly porous thin films," Ph.D. thesis, University of Alberta, 2003.
27. D. J. Elliott, *Integrated Circuit Fabrication Technology*, 2nd ed. (McGraw-Hill, 1989), pp. 62–64.
28. P. Baumeister, *Optical Coating Technology* (SPIE Optical Engineering Press, 2004), pp. 9-56–9-57.
29. L. Gao, F. Lemarchand, M. Lequime, "Refractive index determination of SiO₂ layer in the UV/Vis/NIR range: spectrophotometric reverse engineering on single and bi-layer designs," *J. Eur. Opt. Soc.-Rapid* **8**, 13010 (2013).
30. S. Papernov and A. W. Schmid, "Localized absorption effects during 351 nm, pulsed laser irradiation of dielectric multilayer thin films," *J. Appl. Phys.* **82**, 5422–5432 (1997).

31. S. Papernov, D. Zaksas, J. F. Anzellotti, D. J. Smith, A. W. Schmid, D. R. Collier, and F. A. Carbone, "One step closer to the intrinsic laser-damage threshold of HfO₂ and SiO₂ monolayer thin films," Proc. SPIE **3244**, 434–445 (1998).